IOP Publishing European Journal of Physics
Eur. J. Phys. **44** (2023) 015002 (20pp) https://doi.org/10.1088/1361-6404/ac986b

An analytical, numerical and experimental study of the double pendulum

Serge D'Alessio*

Centre for Education in Mathematics and Computing, Faculty of Mathematics, University of Waterloo, Waterloo, Ontario, N2L 3G1, Canada

E-mail: sdalessio@uwaterloo.ca

Received 27 May 2022, revised 18 September 2022
Accepted for publication 7 October 2022
Published 3 November 2022

Abstract

This investigation takes advantage of the complicated behavior of the double pendulum to highlight some well known techniques that can be used to better understand the dynamics and solutions emerging from this rich problem. Analytical and numerical methods are successfully applied and contrasted to illustrate their usefulness and limitations. This blended analytical-numerical approach to tackling this problem can be an effective resource to physics teachers. The paper should be accessible to upper-year undergraduate physics and mathematics students. Supplemental materials accompanying this work include a MATLAB program to solve the equations of motion and an experimental video; they are included to assist both students and teachers.

Keywords: pendulum, numerical, analytical, chaos, experimental

Supplementary material for this article is available online

(Some figures may appear in colour only in the online journal)

1. Introduction

A pendulum can be defined as a suspended mass that is able to swing freely from a pivot. The simple pendulum, which is a common experiment introduced in high school with historical importance [1], refers to the system consisting of a massless and inextensible rod that is connected to a point-like mass. Although the simple pendulum offers a straightforward approximate relationship between its period and length for small amplitudes of oscillation, the exact relationship for an arbitrary amplitude is more complicated and is typically covered at the university level. In general, any rigid body will swing under its own weight about a fixed point, and this is referred to as a physical pendulum. The spherical pendulum denotes a pendulum

*Author to whom any correspondence should be addressed.

that is free to move on a spherical surface, and the conical pendulum is a special case of a spherical pendulum when the motion is confined to a horizontal plane [2].

There are several important applications associated with pendulums. For example, prior to the advent of electronic timing devices, ballistic pendulums, consisting of a suspended block of wood, were used to measure the speed of bullets [2]. By firing a bullet into the block of wood and measuring the vertical rise of the block, the speed of the bullet can be deduced in terms of the vertical rise, the mass of the bullet, and the mass of the block. In 1798 Henry Cavendish constructed a torsional pendulum and used it as a balance to determine the gravitational constant, $G = 6.67 \times 10^{-11}$ m^3 kg^{-1} s^2, by measuring the angle of rotation of the pendulum caused by the force of attraction between masses [3]. By applying Hooke's law he was able to relate G to the properties of the fiber used to suspend the pendulum. To illustrate the effect of the Coriolis force caused by the Earth's rotation, Jean Foucault in 1851 demonstrated that the pendulum's vertical plane of oscillation precessed at a rate related to the Earth's rotation, $\omega = 2\pi$ radians/day, and latitude of the pendulum [4]. Lastly, Christiaan Huygens near the middle of the 17th century exploited the equal-time property of the brachistochrone to construct a cycloidal pendulum which forced the period of the pendulum to be independent of the amplitude of oscillation, and hence, improved the accuracy of pendulum clocks [4]. These applications along with others are discussed in more detail in a recent video [5].

The focus of the present article is the double pendulum which can be described as one pendulum suspended from another. This continues to be an intriguing problem on several levels [6], and simulations of the double pendulum are readily available on the internet. Experiments involving the double pendulum are usually used to highlight the basic concepts of chaos and sensitivity to initial conditions [7–10]. Numerical simulations provides another means of reinforcing these ideas and has the added benefit of illustrating the importance and role of computation in physics [11, 12]. Further, because the system of equations governing the double pendulum is nonlinear, it offers an opportunity to explore analytical techniques to derive approximate solutions. Numerical simulations and comparisons between some numerical and analytical results are conducted in this study. Although this investigation emphasizes analytical and numerical methods, some experimental results are also included along with the video cited above which features a double compound pendulum.

The paper is structured as follows. In the next section we formulate the problem. Then, in section 3 we present some approximate analytical solutions. A numerical solution procedure is outlined in section 4, and is followed by a brief description of the experiments in section 5. The results are discussed and compared in section 6, and a brief summary is given in the concluding section.

2. Mathematical formulation

Before deriving the governing equations for the double pendulum, we first illustrate the formulation procedure with the simple pendulum shown in figure 1. We consider a mass, m, allowed to swing freely in the absence of friction on the end of a massless inextensible rod of length l which is anchored at the origin in the x–z plane. Here, θ denotes the angle that the rod makes with the vertical, and the vector $\vec{g}$ refers to the acceleration due to gravity having a magnitude denoted by g. In terms of l and θ, the coordinates, velocities and accelerations of the mass are easily obtained with the understanding that a dot represents differentiation with respect to time, t. From the free body diagram shown in figure 2, balancing the forces in the horizontal and vertical directions yields

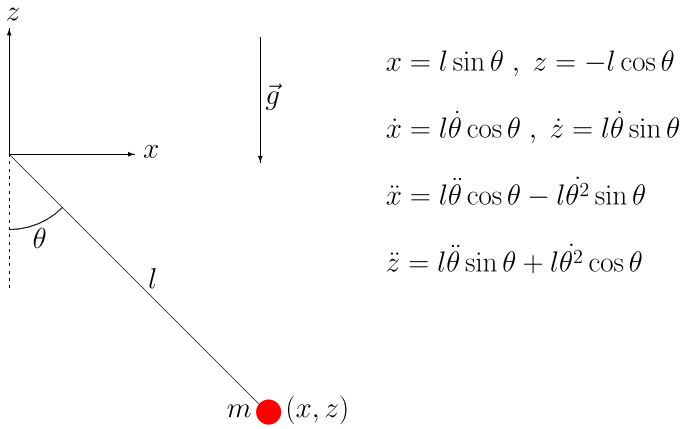

Figure 1. Setup of the simple pendulum.

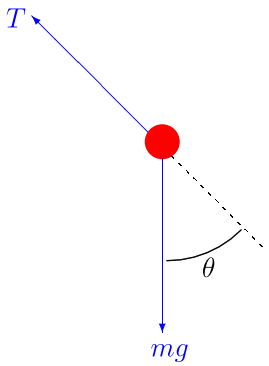

Figure 2. Free body diagram of the simple pendulum.

$$m\ddot{x} = -T\ \sin\ \theta, \qquad m\ddot{z} = T\ \cos\ \theta - mg.$$

We next eliminate the tension, T, by multiplying the first equation by $\cos\theta$ and the second equation by $\sin\theta$ and adding, which leads to

$$\ddot{x}\cos\ \theta + \ddot{z}\ \sin\ \theta = -g\ \sin\ \theta.$$

Substituting the expressions for $\ddot{x}, \ddot{z}$ given in figure 1 then brings us to the familiar differential equation given by

$$\ddot{\theta} + \frac{g}{l}\ \sin\ \theta = 0. \tag{1}$$

Of course, this equation could more easily be obtained by working in terms of polar coordinates. The approach adopted here will be useful when we consider the double pendulum.

For small amplitudes of oscillation we can approximate $\sin\theta$ by θ. Equation (1) then becomes

$$\ddot{\theta} + \frac{g}{l}\theta = 0,$$

and the solution satisfying the initial conditions that the pendulum is released from rest (i.e. $\dot{\theta}(0) = 0$) with amplitude θ_0 (i.e. $\theta(0) = \theta_0$) is easily found to be

$$\theta(t) = \theta_0 \cos\left(\sqrt{\frac{g}{l}}t\right).$$

This approximation is quite reasonable for amplitudes in the range $-10^\circ < \theta < 10^\circ$, and results in simple harmonic motion having a period, P, given by

$$P = \frac{2\pi}{\omega} \quad \text{with } \omega = \sqrt{\frac{g}{l}}, \quad \text{or } P = 2\pi\sqrt{\frac{l}{g}}. \tag{2}$$

Retaining more terms in the expansion for $\sin\theta$ would yield a better approximation and is discussed in [13]. The exact solution to (1) can be obtained by invoking conservation of energy as follows. If the pendulum of mass m is released from rest at an angle θ_0 and we ignore air resistance, then by conservation of energy we have

$$\frac{1}{2}m(l\dot{\theta})^2 + mgl(1 - \cos\,\theta) = mgl(1 - \cos\,\theta_0).$$

Using the trigonometric identity

$$\cos\,\theta = 1 - 2\sin^2\left(\frac{\theta}{2}\right),$$

leads to the equation

$$\dot{\theta}^2 = \frac{4g}{l}\left[\sin^2\left(\frac{\theta_0}{2}\right) - \sin^2\left(\frac{\theta}{2}\right)\right].$$

If we next introduce Φ such that

$$\sin\,\Phi = \frac{1}{k}\sin\left(\frac{\theta}{2}\right) \quad \text{where } k = \sin\left(\frac{\theta_0}{2}\right),$$

then it follows that

$$\dot{\theta}^2 = \left(\frac{4k^2\cos^2\Phi}{1 - k^2\sin^2\Phi}\right)\dot{\Phi}^2,$$

and our equation transforms to

$$\dot{\Phi}^2 = \frac{g}{l}(1 - k^2\sin^2\Phi) \quad \text{or} \quad \frac{\mathrm{d}\Phi}{\mathrm{d}t} = \sqrt{\frac{g}{l}}\sqrt{1 - k^2\sin^2\Phi}.$$

Separating the variables and integrating from $\Phi = 0$ to $\Phi = \pi/2$ (i.e. $\theta = \theta_0$) which corresponds to one quarter of the period, yields an expression for the period given by

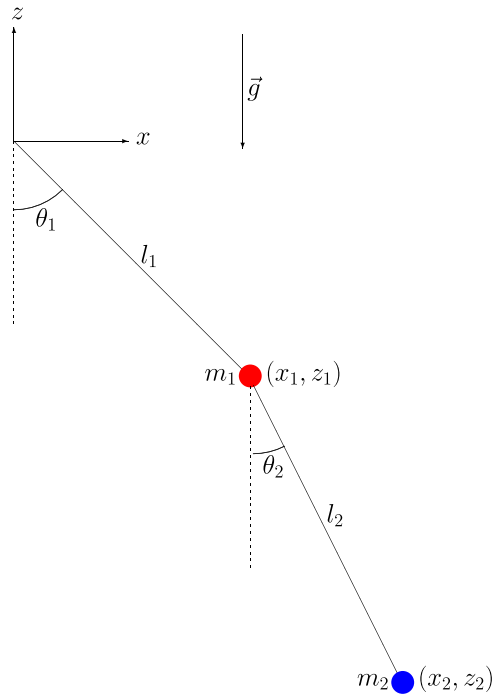

Figure 3. Setup of the double pendulum.

$$P = 4\sqrt{\frac{l}{g}}\int_0^{\pi/2}\frac{\mathrm{d}\Phi}{\sqrt{1-k^2\sin^2\Phi}}.$$

For small amplitude θ_0, $k \approx \theta_0/2$ and we can expand the integrand using the binomial series and integrate term-by-term to obtain

$$P \approx 4\sqrt{\frac{l}{g}}\int_0^{\pi/2}\left(1+\frac{\theta_0^2}{8}\sin^2\Phi+\cdots\right)\mathrm{d}\Phi = 2\pi\sqrt{\frac{l}{g}}\left(1+\frac{\theta_0^2}{16}+\cdots\right).$$

We see that the first term in the above recovers the expression given by (2), while all subsequent terms will add a slight increase to the period.

We now consider the undamped double pendulum with masses m_1 and m_2 and lengths l_1 and l_2 as illustrated in figure 3. Making the same assumptions as with the simple pendulum, the coordinates and accelerations of the masses are given by

$$x_1 = l_1\sin\theta_1, \qquad x_2 = x_1 + l_2\sin\theta_2, \qquad z_1 = -l_1\cos\theta_1, \qquad z_2 = z_1 - l_2\cos\theta_2,$$
$$\ddot{x}_1 = l_1\ddot{\theta}_1\cos\theta_1 - l_1\dot{\theta}_1^2\sin\theta_1, \qquad \ddot{z}_1 = l_1\ddot{\theta}_1\sin\theta_1 + l_1\dot{\theta}_1^2\cos\theta_1,$$
$$\ddot{x}_2 = \ddot{x}_1 + l_2\ddot{\theta}_2\cos\theta_2 - l_2\dot{\theta}_2^2\sin\theta_2, \qquad \ddot{z}_2 = \ddot{z}_1 + l_2\ddot{\theta}_2\sin\theta_2 + l_2\dot{\theta}_2^2\cos\theta_2.$$

Free body diagrams for the top and bottom pendulums along with force balances in the horizontal and vertical directions are shown in figures 4 and 5, respectively. Starting with the bottom pendulum force balance equations, tension T_2 can be eliminated by multiplying the

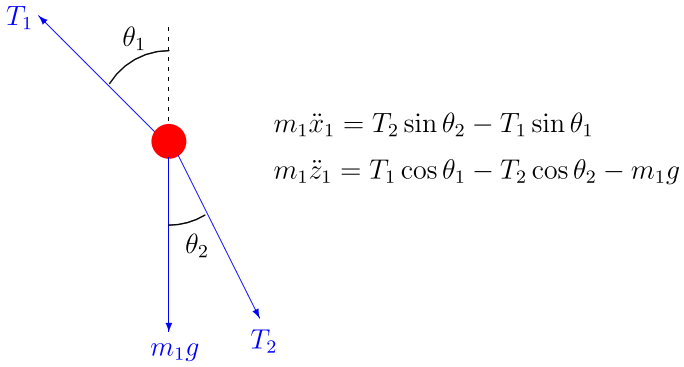

Figure 4. Free body diagram of the top pendulum.

first equation by $\cos\theta_2$ and the second equation by $\sin\theta_2$ and adding. This yields the equation

$$\ddot{x}_2 \cos\theta_2 + \ddot{z}_2 \sin\theta_2 = -g \sin\theta_2.$$

Using the trigonometric identities

$$\cos(\theta_2 - \theta_1) = \cos\theta_2 \cos\theta_1 + \sin\theta_2 \sin\theta_1,$$

$$\sin(\theta_2 - \theta_1) = \sin\theta_2 \cos\theta_1 - \sin\theta_1 \cos\theta_2,$$

it follows that

$$\ddot{x}_2 \cos\theta_2 + \ddot{z}_2 \sin\theta_2 = l_2\ddot{\theta}_2 + l_1\ddot{\theta}_1 \cos(\theta_2 - \theta_1) + l_1\dot{\theta}_1^2 \sin(\theta_2 - \theta_1).$$

Similarly, multiplying the first equation by $-\sin\theta_2$ and the second equation by $\cos\theta_2$ and adding leads to an expression for T_2 given by

$$T_2 = m_2 g \cos\theta_2 + m_2\ddot{z}_2 \cos\theta_2 - m_2\ddot{x}_2 \sin\theta_2.$$

Lastly, substituting the expressions for $\ddot{x}_2, \ddot{z}_2$, followed by the expressions for $\ddot{x}_1, \ddot{z}_1$, then brings us to the following equations

$$l_2\ddot{\theta}_2 + l_1\ddot{\theta}_1 \cos(\theta_2 - \theta_1) + l_1\dot{\theta}_1^2 \sin(\theta_2 - \theta_1) = -g \sin\theta_2, \tag{3}$$

$$T_2 = m_2 g \cos\theta_2 + m_2 l_1\dot{\theta}_1^2 \cos(\theta_2 - \theta_1) + m_2 l_2\dot{\theta}_2^2 - m_2 l_1\ddot{\theta}_1 \sin(\theta_2 - \theta_1). \tag{4}$$

Turning now to the top pendulum force balance equations and applying a similar procedure to eliminate the tension T_1 leads to the equation

$$m_1\ddot{x}_1 \cos\theta_1 + m_1\ddot{z}_1 \sin\theta_1 = T_2 \sin(\theta_2 - \theta_1) - m_1 g \sin\theta_1.$$

Noting that $\ddot{x}_1 \cos\theta_1 + \ddot{z}_1 \sin\theta_1 = l_1\ddot{\theta}_1$ and substituting the above known expression for T_2 we arrive at the following equation

$$l_1[m_1 + m_2 \sin^2(\theta_2 - \theta_1)]\ddot{\theta}_1 - m_2 l_1 \sin(\theta_2 - \theta_1)\cos(\theta_2 - \theta_1)\dot{\theta}_1^2 + m_1 g \sin\theta_1$$
$$= m_2 \sin(\theta_2 - \theta_1)[l_2\dot{\theta}_2^2 + g \cos\theta_2]. \tag{5}$$

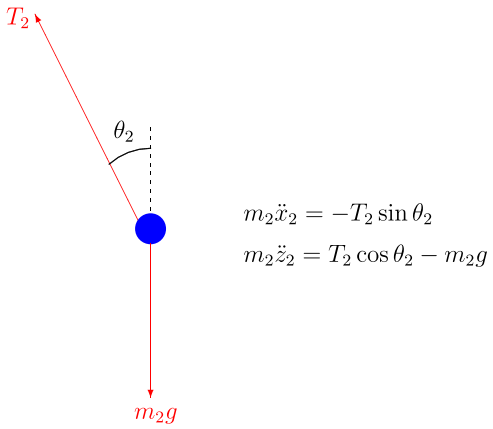

Figure 5. Free body diagram of the bottom pendulum.

Thus, the governing equations for the double pendulum can be rewritten in the following form

$$\left(1 + \frac{m_2}{m_1}\sin^2(\theta_2 - \theta_1)\right)\ddot{\theta}_1 - \frac{m_2}{m_1}\sin(\theta_2 - \theta_1)\cos(\theta_2 - \theta_1)\dot{\theta}_1^2 + \frac{g}{l_1}\sin\theta_1$$
$$= \frac{m_2}{m_1}\sin(\theta_2 - \theta_1)\left(\frac{l_2}{l_1}\dot{\theta}_2^2 + \frac{g}{l_1}\cos\theta_2\right), \tag{6}$$

$$\ddot{\theta}_2 + \frac{g}{l_2}\sin\theta_2 = -\frac{l_1}{l_2}(\sin(\theta_2 - \theta_1)\dot{\theta}_1^2 + \cos(\theta_2 - \theta_1)\ddot{\theta}_1). \tag{7}$$

3. Approximate analytical solutions

Prior to pursuing analytical work it is customary to first cast the governing equations (6) and (7) in dimensionless form. To achieve this we introduce the following parameters

$$M = \frac{m_2}{m_1}, \qquad L = \frac{l_2}{l_1}, \qquad \tau = \sqrt{\frac{g}{l_1}}t, \qquad \Delta\theta = \theta_2 - \theta_1,$$

where the quantities M and L denote the dimensionless mass and length ratios, τ denotes the dimensionless time, and $\Delta\theta$ refers to the change between the angular displacements θ_2 and θ_1. Then, the dimensionless equations now become

$$(1 + M\sin^2(\Delta\theta))\theta_1'' - \frac{M}{2}\sin(2\Delta\theta)(\theta_1')^2 + \sin\theta_1$$
$$= M\sin(\Delta\theta)(L(\theta_2')^2 + \cos\theta_2), \tag{8}$$

$$L\theta_2'' + \sin\theta_2 = -\sin(\Delta\theta)(\theta_1')^2 - \cos(\Delta\theta)\theta_1''. \tag{9}$$

Here, the prime is used to designate differentiation with respect to τ. Equations (8) and (9) represent a nonlinear coupled system of second-order differential equations that is too complicated to solve exactly. Instead, approximate solutions will be explored in this section.

If we restrict ourselves to small amplitudes of oscillation about the vertical, then we can make the following approximations $\sin\theta \approx \theta$ and $\cos\theta \approx 1$. Further, all terms involving non-linear products will be much smaller than linear terms, and hence, can be ignored. Doing this yields the following linearized system of differential equations

$$\theta_1'' + (1+M)\theta_1 = M\theta_2, \tag{10}$$

$$L\theta_2'' + \theta_2 = -\theta_1''. \tag{11}$$

These equations can easily be combined into a single fourth-order linear differential equation given by

$$L\theta_2'''' + (1+M)(1+L)\theta_2'' + (1+M)\theta_2 = 0. \tag{12}$$

If we assume a solution of the form $\theta_2(\tau) = A\cos(\omega\tau + B)$, where A and B are arbitrary constants, then the frequency ω must satisfy the quadratic equation in ω^2

$$L(\omega^2)^2 - (1+M)(1+L)\omega^2 + (1+M) = 0, \tag{13}$$

and the following solutions emerge

$$\omega_\pm^2 = \frac{(1+M)(1+L) \pm \sqrt{(1+M)^2(1+L)^2 - 4L(1+M)}}{2L}. \tag{14}$$

The solution for θ_1 can then be determined by solving (10) from which it follows that

$$\theta_2 = \left(\frac{1+M-\omega_\pm^2}{M}\right)\theta_1.$$

Hence, if the sign of $(1+M-\omega_\pm^2)$ is positive, then the pendulums are oscillating in-phase, otherwise they are out-of-phase. Although the sign will depend on the values of the parameters M and L, after some algebra it can be shown that

$$1+M-\omega_\pm^2 = (1+M)(1-L) \mp \sqrt{(1+M)^2(1-L)^2 + 4LM(1+M)}.$$

Expressed this way, it is clear that for all values of M and L, the frequency ω_+ corresponds to the out-of-phase (or antisymmetric) mode of vibration, while ω_- corresponds to the in-phase (or symmetric) mode of vibration.

We next illustrate an advantage of rendering the equations in dimensionless form by investigating two limiting cases. The first corresponds to the case when $m_1 \gg m_2$, or equivalently $M \ll 1$. In this limit we can make the approximation $M \approx 0$ in equations (8) and (9) and obtain

$$\theta_1'' + \sin\,\theta_1 = 0, \tag{15}$$

$$L\theta_2'' + \sin\,\theta_2 = -\sin(\Delta\theta)(\theta_1')^2 - \cos(\Delta\theta)\theta_1''. \tag{16}$$

The effect of having a much heavier top mass is that the equations become decoupled; that is, equation (15) does not involve θ_2, and thus, in theory can be solved for θ_1 and then substituted into (16) to obtain θ_2. In fact, equation (15) is the dimensionless form of equation (1) which indicates that the top pendulum behaves like a simple pendulum. Equation (16) then describes a forced simple pendulum. For small amplitudes the top pendulum oscillates with a

dimensionless frequency $\omega = 1$ and dimensionless period $P = 2\pi$. This is in agreement with equation (14), since setting $M = 0$ yields $\omega_- = 1$. Equation (16) can also be linearized to give

$$L\theta_2'' + \theta_2 = -\theta_1''.$$

If we assume that both pendulums are released from rest with initial amplitudes $\theta_{1,0}, \theta_{2,0}$, then $\theta_1(\tau) = \theta_{1,0}\cos(\tau)$, and the solution to the above equation becomes

$$\theta_2(\tau) = \left(\theta_{2,0} - \frac{\theta_{1,0}}{1-L}\right)\cos\left(\frac{\tau}{\sqrt{L}}\right) + \frac{\theta_{1,0}}{1-L}\cos(\tau) \quad \text{for } L \neq 1.$$

We note that we must avoid $L = 1$ since this would lead to resonance which will violate the small amplitude assumption. Also, we observe that the frequency $\omega = 1/\sqrt{L}$ corresponds to ω_+ from equation (14) when $M = 0$. Thus, for $M \ll 1$ the two pendulums are decoupled with the top pendulum oscillating with natural frequency $\omega_- = 1$ and the bottom pendulum oscillating with natural frequency $\omega_+ = 1/\sqrt{L}$.

Another limiting case occurs when $L \gg 1$. In this limit we can make the approximation $\frac{1}{L} \approx 0$ after dividing equations (8) and (9) by L. The system then reduces to $(\theta_2')^2 = 0$ and $\theta_2'' = 0$ which admits the solution $\theta_2(\tau) = C$ where C is an arbitrary constant. For large L the roots of equation (14) are found to be $\omega_- = 0$ and $\omega_+ = \sqrt{1+M}$. Once again the pendulums become decoupled. This time the bottom pendulum is stationary since $\omega_- = 0$, and thus, we can set the arbitrary constant $C = 0$. This finding is consistent with equation (2) since $\omega = \sqrt{g/l} \to 0$ as $l \to \infty$. Setting $\theta_2 = 0$ in equation (8) and linearizing leads to

$$\theta_1'' + (1+M)\theta_1 = 0,$$

which reveals that the top pendulum oscillates with natural frequency $\omega_+ = \sqrt{1+M}$ in accordance with equation (14).

We end this section by outlining a formal procedure for constructing an approximate solution to equations (8) and (9) valid for small amplitudes of oscillation. As we will shortly see, this technique will reproduce the results obtained earlier in this section. This technique is known as the method of multiple scales [14]. This method tackles equations possessing multiple time scales by introducing slow and fast time variables. We begin by defining two time scales: $\tau_0 = \tau$ and $\tau_1 = \epsilon\tau$ where $0 < \epsilon \ll 1$ is a small parameter. In addition, for small amplitudes of oscillation we can set $\theta_1 = \epsilon\phi$, $\theta_2 = \epsilon\psi$ and expand the following quantities in a series in powers of ϵ

$$\sin\,\theta_1 = \sin(\epsilon\phi) = \epsilon\phi + \cdots, \qquad \sin\,\theta_2 = \sin(\epsilon\psi) = \epsilon\psi + \cdots,$$

$$\sin(2\Delta\theta) = \sin(2\epsilon(\psi-\phi)) = 2\epsilon(\psi-\phi) + \cdots,$$

$$\sin^2(\Delta\theta) = \sin^2(\epsilon(\psi-\phi)) = \epsilon^2(\psi-\phi)^2 + \cdots,$$

$$\cos(\Delta\theta) = \cos(\epsilon(\psi-\phi)) = 1 - \frac{\epsilon^2}{2}(\psi-\phi)^2 + \cdots.$$

Lastly, we also expand ϕ and ψ in a series in powers of ϵ

$$\phi = \phi_0 + \epsilon\phi_1 + \cdots, \qquad \psi = \psi_0 + \epsilon\psi_1 + \cdots.$$

In terms of the time variables τ_0 and τ_1 the derivatives of a generic quantity

$$\chi = \chi_0 + \epsilon\chi_1 + \cdots,$$

(with $\chi = \phi$ or $\chi = \psi$) become

$$\chi' = \frac{\mathrm{d}\chi}{\mathrm{d}\tau} = \frac{\partial \chi_0}{\partial \tau_0} + \epsilon\left(\frac{\partial \chi_0}{\partial \tau_1} + \frac{\partial \chi_1}{\partial \tau_0}\right) + \cdots,$$
$$\chi'' = \frac{\mathrm{d}^2\chi}{\mathrm{d}\tau^2} = \frac{\partial^2 \chi_0}{\partial \tau_0^2} + \epsilon\left(2\frac{\partial^2 \chi_0}{\partial \tau_0 \partial \tau_1} + \frac{\partial^2 \chi_1}{\partial \tau_0^2}\right) + \cdots.$$

When these series are substituted into equations (8) and (9), a hierarchy of problems at various orders of ϵ are obtained. The leading-order problem is given by the following coupled system of linear partial differential equations

$$\frac{\partial^2 \phi_0}{\partial \tau_0^2} + (1+M)\phi_0 = M\psi_0, \tag{17}$$
$$L\frac{\partial^2 \psi_0}{\partial \tau_0^2} + \psi_0 = -\frac{\partial^2 \phi_0}{\partial \tau_0^2}. \tag{18}$$

This system bears a close resemblance to the system given by (10) and (11), and can be solved using a similar approach. We first combine (17) and (18) to obtain

$$L\frac{\partial^4 \psi_0}{\partial \tau_0^4} + (1+M)(1+L)\frac{\partial^2 \psi_0}{\partial \tau_0^2} + (1+M)\psi_0 = 0.$$

The solution is easily shown to be

$$\psi_0(\tau_0, \tau_1) = A(\tau_1)\cos(\omega\tau_0 + B(\tau_1)),$$

where ω satisfies equation (13), and hence, has roots given by (14). The main difference here is that A, B are not arbitrary constants, but rather arbitrary functions of τ_1. The solution for ϕ_0 can be obtained by solving (17). By proceeding to the $O(\epsilon)$ problem we will show that A, B are indeed constants and not functions. The $O(\epsilon)$ problem is governed by

$$\frac{\partial^2 \phi_1}{\partial \tau_0^2} + (1+M)\phi_1 - M\psi_1 = -2\frac{\partial^2 \phi_0}{\partial \tau_0 \partial \tau_1}, \tag{19}$$
$$L\frac{\partial^2 \psi_1}{\partial \tau_0^2} + \psi_1 + \frac{\partial^2 \phi_1}{\partial \tau_0^2} = -2\frac{\partial^2}{\partial \tau_0 \partial \tau_1}(\phi_0 + L\psi_0). \tag{20}$$

Now, in order for ϕ_1, ψ_1 to remain bounded we must set the right-hand-sides of (19) and (20) to zero since they represent forcing terms that will give rise to resonance. This immediately leads us to

$$\frac{\partial^2 \psi_0}{\partial \tau_0 \partial \tau_1} = -\frac{\mathrm{d}A}{\mathrm{d}\tau_1}\sin(\omega\tau_0 + B(\tau_1)) - \frac{\mathrm{d}B}{\mathrm{d}\tau_1}\cos(\omega\tau_0 + B(\tau_1)) = 0.$$

In order for this to hold for all τ_0 we require that

$$\frac{\mathrm{d}A}{\mathrm{d}\tau_1} = \frac{\mathrm{d}B}{\mathrm{d}\tau_1} = 0,$$

and hence, A, B are constants. Thus, this approach yields the same solution previously obtained.

Although it may appear more complicated, it provides a systematic procedure for obtaining better approximations. However, the problems get more detailed as we proceed to higher orders of ϵ.

4. Numerical method

We next present a numerical solution procedure to solve the system of equations (8) and (9). We begin by rewriting equations (8) and (9) as a first-order system of autonomous coupled differential equations by defining $U = \theta_1'$ and $V = \theta_2'$. Then system (8) and (9) can be expressed as

$$\frac{\mathrm{d}\theta_1}{\mathrm{d}\tau} = F_1(U), \tag{21}$$

$$\frac{\mathrm{d}U}{\mathrm{d}\tau} = F_2(\theta_1, U, \theta_2, V), \tag{22}$$

$$\frac{\mathrm{d}\theta_2}{\mathrm{d}\tau} = F_3(V), \tag{23}$$

$$\frac{\mathrm{d}V}{\mathrm{d}\tau} = F_4(\theta_1, U, \theta_2, V), \tag{24}$$

where

$$F_1(U) = U,$$

$$F_2(\theta_1, U, \theta_2, V) = \frac{M\,\sin(\theta_2 - \theta_1)[LV^2 + \cos\,\theta_2] + \frac{M}{2}\,\sin[2(\theta_2 - \theta_1)]U^2 - \sin\,\theta_1}{1 + M\sin^2(\theta_2 - \theta_1)},$$

$$F_3(V) = V,$$

$$F_4(\theta_1, U, \theta_2, V) = -\frac{1}{L}\,\sin\,\theta_2 - \frac{1}{L}\,\sin(\theta_2 - \theta_1)U^2 - \frac{1}{L}\,\cos(\theta_2 - \theta_1)F_2(\theta_1, \theta_2, U, V).$$

To numerically solve equations (21)–(24) the fourth-order Runge–Kutta (RK4) algorithm [15] was adopted because of its simplicity, accuracy and popularity. When applied to the system (21)–(24) the RK4 method advances the solution from time τ_n to time $\tau_{n+1} = \tau_n + \Delta\tau$ according to the following marching algorithm

$$\theta_{1,n+1} = \theta_{1,n} + \frac{\Delta\tau}{6}(K_1 + 2K_2 + 2K_3 + K_4),$$

$$U_{n+1} = U_n + \frac{\Delta\tau}{6}(L_1 + 2L_2 + 2L_3 + L_4),$$

$$\theta_{2,n+1} = \theta_{2,n} + \frac{\Delta\tau}{6}(M_1 + 2M_2 + 2M_3 + M_4),$$

$$V_{n+1} = V_n + \frac{\Delta\tau}{6}(N_1 + 2N_2 + 2N_3 + N_4),$$

where

$$K_1 = F_1(U_n), \qquad L_1 = F_2(\theta_{1,n}, U_n, \theta_{2,n}, V_n),$$

$$M_1 = F_3(V_n), \qquad N_1 = F_4(\theta_{1,n}, U_n, \theta_{2,n}, V_n),$$

$$K_2 = F_1\left(U_n + \frac{L_1\Delta\tau}{2}\right),$$

$$L_2 = F_2\left(\theta_{1,n} + \frac{K_1\Delta\tau}{2}, U_n + \frac{L_1\Delta\tau}{2}, \theta_{2,n} + \frac{M_1\Delta t}{2}, V_n + \frac{N_1\Delta\tau}{2}\right),$$

$$M_2 = F_3\left(V_n + \frac{N_1\Delta\tau}{2}\right),$$

$$N_2 = F_4\left(\theta_{1,n} + \frac{K_1\Delta\tau}{2}, U_n + \frac{L_1\Delta\tau}{2}, \theta_{2,n} + \frac{M_1\Delta t}{2}, V_n + \frac{N_1\Delta\tau}{2}\right),$$

$$K_3 = F_1\left(U_n + \frac{L_2\Delta\tau}{2}\right),$$

$$L_3 = F_2\left(\theta_{1,n} + \frac{K_2\Delta\tau}{2}, U_n + \frac{L_2\Delta\tau}{2}, \theta_{2,n} + \frac{M_2\Delta t}{2}, V_n + \frac{N_2\Delta\tau}{2}\right),$$

$$M_3 = F_3\left(V_n + \frac{N_2\Delta\tau}{2}\right),$$

$$N_3 = F_4\left(\theta_{1,n} + \frac{K_2\Delta\tau}{2}, U_n + \frac{L_2\Delta\tau}{2}, \theta_{2,n} + \frac{M_2\Delta t}{2}, V_n + \frac{N_2\Delta\tau}{2}\right),$$

$$K_4 = F_1(U_n + L_3\Delta\tau),$$

$$L_4 = F_2\big(\theta_{1,n} + K_3\Delta\tau, U_n + L_3\Delta\tau, \theta_{2,n} + M_3\Delta t, V_n + N_3\Delta\tau\big),$$

$$M_4 = F_3(V_n + N_3\Delta\tau),$$

$$N_4 = F_4\big(\theta_{1,n} + K_3\Delta\tau, U_n + L_3\Delta\tau, \theta_{2,n} + M_3\Delta t, V_n + N_3\Delta\tau\big).$$

Here, $\theta_{1,n}, U_n, \theta_{2,n}, V_n$ are the computed solutions at time τ_n while $\theta_{1,n+1}, U_{n+1}, \theta_{2,n+1}, V_{n+1}$ are the sought after solutions at time τ_{n+1}. We note that for the special case consisting of a single first-order differential equation where the right-hand-side function depends only on τ, the RK4 algorithm reduces to evaluating an integral using Simpson's rule. In our simulations a time step of $\Delta t = 0.005$ was used. The MATLAB program (titled 'DoublePendulum.m') used to solve the above system of equations is provided as supplemental material [16].

5. Experimental details

Experiments were conducted using the double pendulum shown in figure 6 which consisted of three aluminum flat bars hinged together as illustrated in the diagrams. As seen in the photographs, the double pendulum was constructed by attaching two physical pendulums together end to end. The bar dimensions were 38 × 6 mm with two of the bars having lengths of 205 mm while the third bar, which swings between the two longer bars, had a length of 180 mm. Each of the top bars had a mass 124 g while the bottom bar had a mass of 110 g. The distance between the pivots was 173 mm and the distance from the bottom pivot to the bottom edge of the bar was 163 mm. Rotational friction was minimized by using stainless steel bearings as the hinging mechanism. The double pendulum is connected to a small plate which enabled it to be mounted to a supporting wall or a piece of wood.

Figure 6. Three dimensional and side view of the double compound pendulum.

The experimental apparatus described above was used to illustrate and reinforce various concepts. First, when the two pendulums forming the double pendulum were released from small initial angles with the vertical, in-phase and out-of-phase periodic oscillations were observed depending on the relative signs of the initial angles as predicted in section 3. On the other hand, when the initial angles were large the motion was no longer periodic and quickly became unpredictable.

Sensitivity to initial conditions is a characteristic feature of chaos. This distinctive feature of chaos was visualized by arranging two double pendulums in tandem. This was accomplished by mounting one double pendulum in front of the other. When the double pendulums were released from the same small initial angles the two double pendulums were observed to oscillate synchronously for a long period of time. However, when they were released from large initial angles the paths of the two double pendulums quickly diverged from each other despite the attempts to have them exactly aligned at the start.

The observations described in this section are captured in the video [5] provided, and are also illustrated in the numerical simulations reported in the next section.

6. Results and discussion

In this section we discuss some numerical simulations that were conducted and validate some of the analytical predictions made in section 3. Here, we have used the parameter values

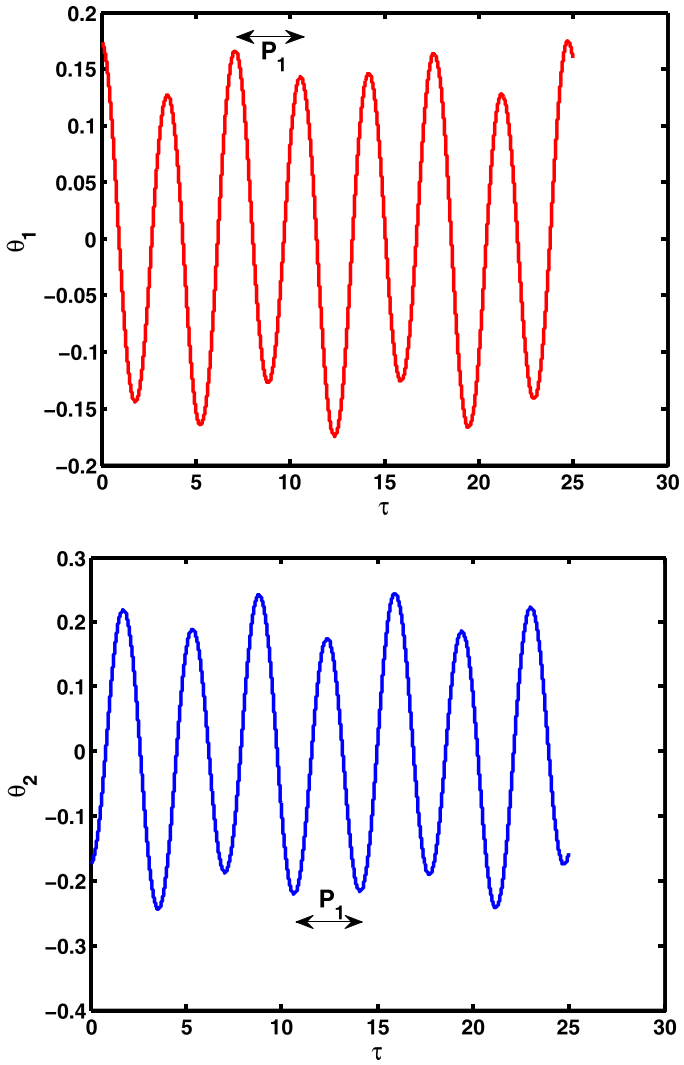

Figure 7. Out-of-phase case with $L = M = 1$, $\alpha = \frac{\pi}{18}$ and $\beta = -\frac{\pi}{18}$.

$M = L = 1$ for all the numerical results presented. We begin with some simulations involving small amplitudes of oscillation. As already explained, the linearized equations represent a reasonable approximation to the fully nonlinear equations, and predicted two natural frequencies given by (14). With $L = M = 1$ these frequencies are

$$\omega_1 = \omega_+ = \sqrt{2+\sqrt{2}} \approx 1.85 \quad \text{and} \quad \omega_2 = \omega_- = \sqrt{2-\sqrt{2}} \approx 0.77,$$

and can be associated with the out-of-phase and in-phase modes of vibration, respectively. The periods corresponding to these frequencies are

$$P_1 = \frac{2\pi}{\omega_1} \approx 3.40 \quad \text{and} \quad P_2 = \frac{2\pi}{\omega_2} \approx 8.21.$$

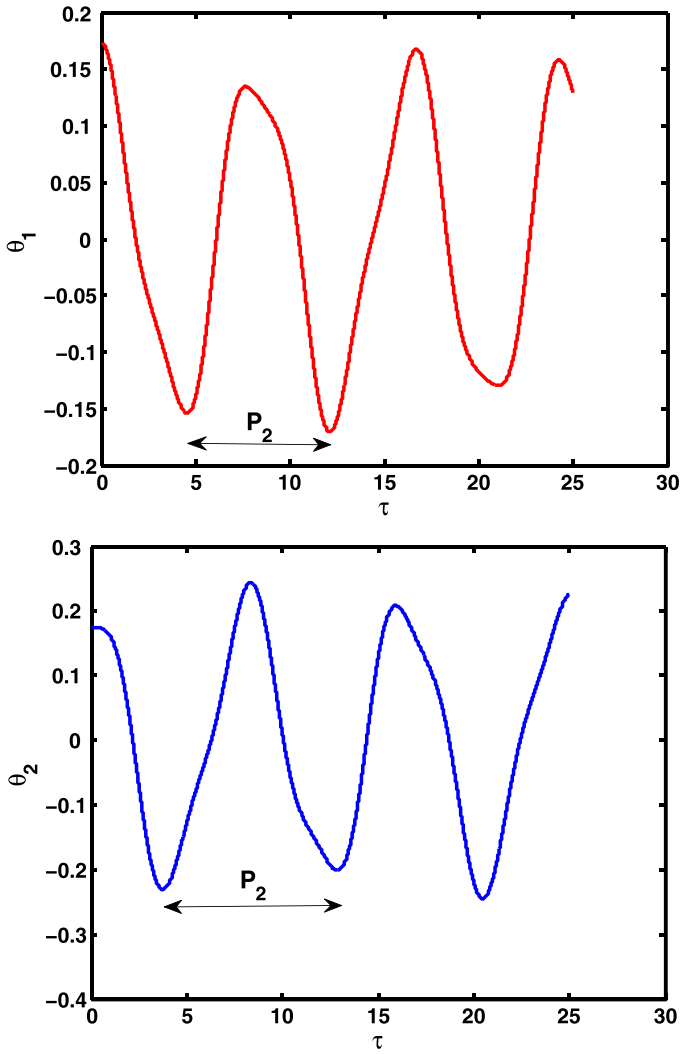

Figure 8. In-phase case with $L = M = 1$ and $\alpha = \beta = \frac{\pi}{18}$.

To verify this, simulations were carried out whereby the fully nonlinear equations (8) and (9) were numerically solved subject to small amplitudes of oscillation. Shown in figure 7 are time variations of θ_1 (top diagram) and θ_2 (bottom diagram) for an out-of-phase simulation where the pendulums were released from rest with initial amplitudes of $\theta_1(0) = \alpha = \frac{\pi}{18}$ radians, or 10°, and $\theta_2(0) = \beta = -\frac{\pi}{18}$ radians, or -10°. These plots reveal fluctuations that appear to be periodic with a period that is close to P_1. Figure 8 illustrates an in-phase simulation where the pendulums were released from rest with initial amplitudes of $\theta_1(0) = \alpha = \frac{\pi}{18}$ radians, or 10°, and $\theta_2(0) = \beta = \frac{\pi}{18}$ radians, or 10°. This time the observed period is close to P_2. Thus, we see from these simulations that the fully nonlinear equations (8) and (9) are well approximated by the linearized set of equations (10) and (11) for small amplitudes of oscillation.

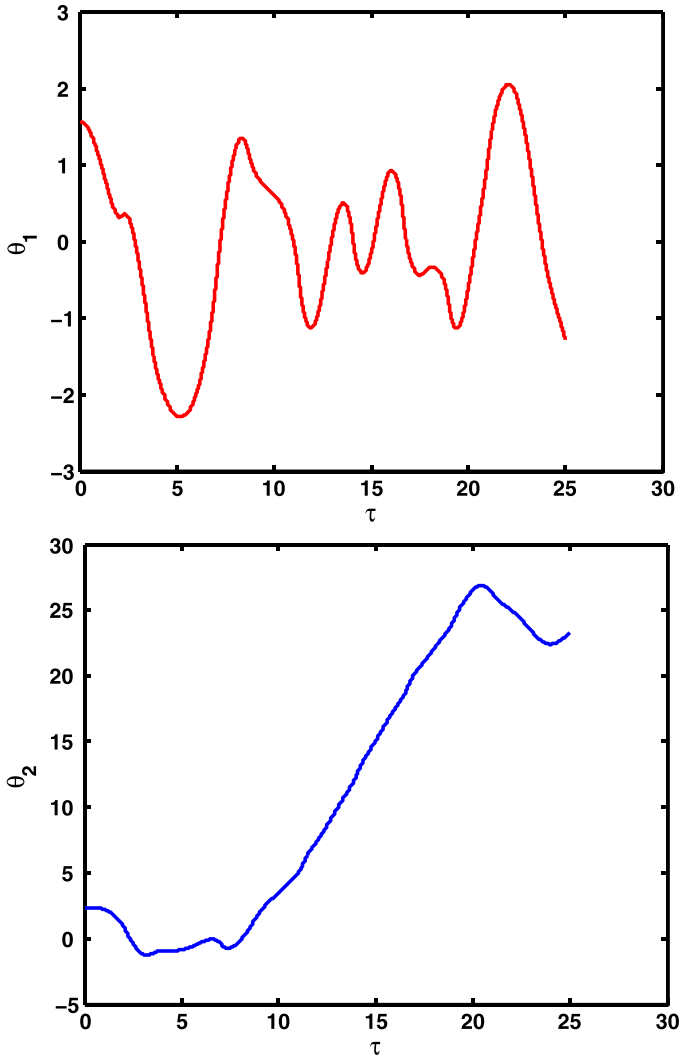

Figure 9. Angular displacements for the case $L = M = 1$, $\alpha = \frac{\pi}{2}$ and $\beta = \frac{3\pi}{4}$.

Experiments were also conducted with small amplitudes of oscillation. The difficulty in making comparisons between the experiments and the analyses arises from the fact that the experiments involved a double compound (i.e. physical) pendulum while the mathematical model, and hence numerical simulations, was formulated for a simple double pendulum. In order to correct for this we made use of the following result. As previously noted, the period for a simple pendulum executing a small amplitude of oscillation is given by

$$P = 2\pi\sqrt{\frac{l}{g}},$$

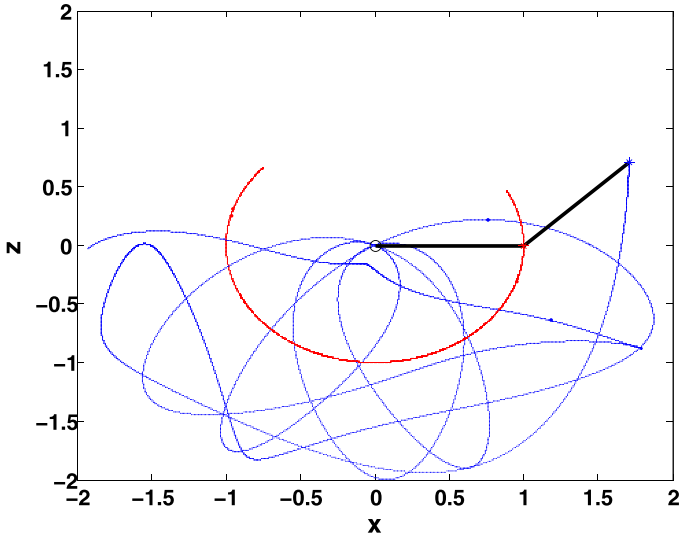

Figure 10. Trajectories for the case $L = M = 1$, $\alpha = \frac{\pi}{2}$ and $\beta = \frac{3\pi}{4}$.

while for a physical pendulum the corresponding expression for the period can be shown to be [3]

$$P = 2\pi\sqrt{\frac{I}{mgD}},$$

where I denotes the moment of inertia about the point of suspension and D is the linear distance from the point of suspension to the center of mass. For a uniform bar of length l the above simplifies to [3]

$$P = 2\pi\sqrt{\frac{2l}{3g}}. \tag{25}$$

Before discussing the experimental out-of-phase and in-phase modes of vibration of the double compound pendulum we first compared how our experiments agreed with equation (25). To do this we removed the bottom pendulum by simply disconnecting the bottom bar shown in figure 6. Using the data from the previous section equation (25) yields a period of $P \approx 0.68$ s which agreed well with the measured period of 0.74 s. Equipped with this we then computed the out-of-phase and in-phase periods predicted by equation (14) for the double compound pendulum. Using the data from the previous section it follows that $L = 0.94$ and $M = 0.44$, and the dimensionless out-of-phase and in-phase periods are $P_1 \approx 2.72$ and $P_2 \approx 9.38$, respectively. Then to convert to dimensional periods, rather than multiplying by $\sqrt{l_1/g}$ we made use of (25) to account for the physical pendulum and multiplied by $\sqrt{2l_1/3g}$. This yields $P_1 \approx 0.29$ s and $P_2 \approx 1.02$ s. After releasing the double compound pendulum several times from small initial angles and recording the periods, the average in-phase period was found to be 0.94 s. Unfortunately, the out-of-phase period was too small to measure accurately with the equipment available. Overall, the agreement between the theoretical and observed in-phase period is reasonable given the approximation made. And since we already demonstrated that the numerical

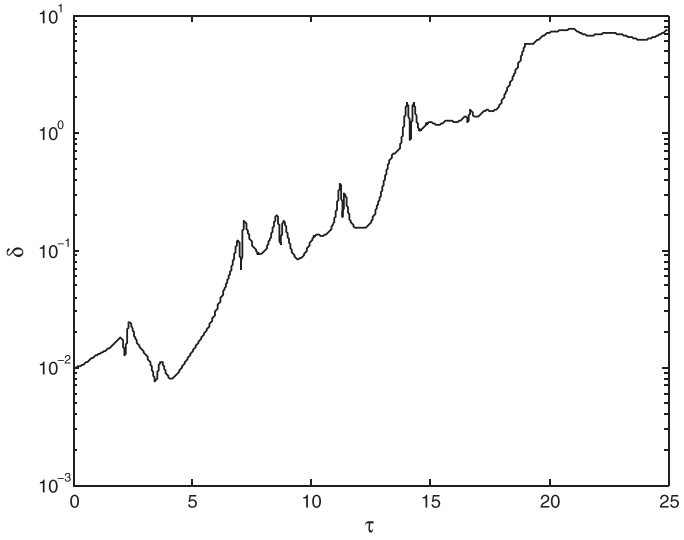

Figure 11. Separation between nearby trajectories with time.

simulations are in good agreement with the analysis, this shows indirectly that there is reasonable agreement between the numerical simulations and the experiments for small amplitudes of oscillation. For large amplitudes of oscillation this quantitative approach is not possible, and we resort to qualitative comparisons as presented in the video [5].

We next consider a case where the initial amplitudes are not small. Portrayed in figure 9 are time variations of θ_1 (top diagram) and θ_2 (bottom diagram) for a simulation where the pendulums were released from rest with initial amplitudes of $\theta_1(0) = \alpha = \frac{\pi}{2}$ radians, or 90°, and $\theta_2(0) = \beta = \frac{3\pi}{4}$ radians, or 135°. Unlike the previous plots, there is no apparent period associated with the motion. Further, the variations in the angular displacements appear to be unpredictable. These are signatures of chaotic motion which is also suggested by the paths traced out by the pendulums demonstrated in figure 10. The trajectory of the bottom pendulum is shown in blue while that of the top pendulum is shown in red. The initial positions of the pendulums are represented by the black lines, and the trajectories plotted span the time interval $0 \leqslant \tau \leqslant 25$. As expected, the top pendulum will follow a circular path whereas the path of the bottom pendulum appears to be chaotic. Another signature of chaotic motion is shown in figure 11 which illustrates on a semilog scale how the separation, δ, between nearby initial conditions seem to diverge exponentially in phase space as time evolves. As noted in the previous section, this behaviour is referred to as sensitivity to initial conditions. In this simulation two trajectories released from rest at the same time were computed simultaneously: one having initial conditions $\theta_1(0) = \frac{\pi}{2}$, $\theta_2(0) = \frac{3\pi}{4}$, $\theta_1'(0) = \theta_2'(0) = 0$, and the second having initial conditions $\theta_1(0) = \frac{\pi}{2} + \delta_0$, $\theta_2(0) = \frac{3\pi}{4}$, $\theta_1'(0) = \theta_2'(0) = 0$. Here, $\delta_0 = 0.01$ denotes the initial separation between the trajectories. The separation was then computed at each time step using the Euclidean distance in phase space $(\theta_1, U = \theta_1', \theta_2, V = \theta_2')$. The motion of the magnetic pendulum reported in [17] also displays a similar behaviour, as does the motion of an inverted pendulum discussed in [18].

We next verify that the motion is indeed chaotic by computing the Lyapunov exponents, λ_i, associated with the exponentially diverging trajectories discussed above. Since our phase space is four-dimensional, $i = 1, \ldots, 4$ and we order the exponents so that λ_1 is the largest and

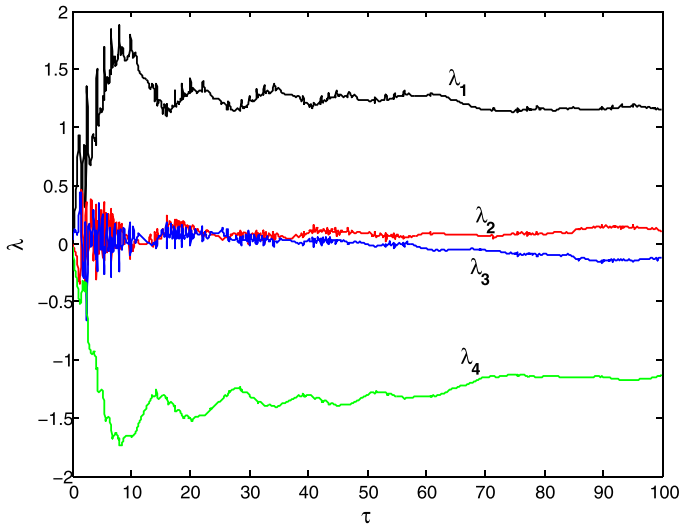

Figure 12. Convergence of the Lyapunov exponents.

λ_4 is the smallest. The double pendulum system is described as being chaotic if at least one Lyapunov exponent is positive. To compute the Lyapunov exponents the algorithm outlined in [19] was utilized. This involved simultaneously solving the system (21)–(24) along with four copies of the corresponding linearized system. The linearized system was used to compute the evolution of small displacements about a point in phase space; the initial conditions were chosen to be a set of 4 orthonormal vectors which form the axes of a four-dimensional sphere. With time these vectors deform and diverge in magnitude, and will tend to follow the direction of most rapid growth. Thus, the four-dimensional sphere becomes a four-dimensional ellipsoid, and the lengths of the principal axes, $p_i(\tau)$, of the ellipsoid are related to the Lyapunov exponents through the relation

$$\lambda_i = \lim_{\tau\to\infty} \frac{1}{\tau} \log_2\left(\frac{p_i(\tau)}{p_i(0)}\right).$$

The Gram–Schmidt orthonormalization procedure was then employed to construct new orthonormal bases as time progressed. Figure 12 displays the output from this calculation using the initial conditions

$$\theta_1(0) = \frac{\pi}{2}, \qquad U(0) = 0, \qquad \theta_2(0) = \frac{3\pi}{4}, \qquad V(0) = 0.$$

Convergence in the values of the four Lyapunov exponents with time is evident in the diagram. Although the plot shows the convergence over the interval $0 \leqslant \tau \leqslant 100$, the calculation was carried out to $\tau = 10\,000$ since the convergence was observed to be slow. The converged values were found to be $\lambda_1 \approx 0.75$, $\lambda_2 \approx 0.28$, $\lambda_3 \approx -0.28$, $\lambda_4 \approx -0.75$. Since $\lambda_1 > 0$, this confirms that the motion illustrated in figures 9–11 is chaotic. Lastly, we note that the four Lyapunov exponents sum to zero; this is because the undamped double pendulum is a conservative system [20], and thus, the volume defined by the principal axes (which grows like $2^{(\lambda_1+\lambda_2+\lambda_3+\lambda_4)\tau}$) remains constant.

7. Summary

This paper applied some analytical and numerical methods to solve for the motion of the double pendulum. New results are presented and discussed which complement our understanding of this problem. Although this was largely an analytical and numerical study, some experimental results involving a double compound pendulum were discussed and presented in the video [5] which is added as supplemental material. Lastly, this work also emphasizes the importance and joint roles of computation, analysis and experiment, which are powerful and effective tools in physics education.

Acknowledgments

The author wishes to thank Zak Holdsworth for building the double pendulum and providing the photos.

ORCID iDs

Serge D'Alessio https://orcid.org/0000-0002-0350-4672

References

[1] Nelson R A and Olsson M G 1986 The pendulum-Rich physics from a simple system *Am. J. Phys.* **54** 112–21
[2] Halliday D and Resnick R 1988 *Fundamentals of Physics* 3rd edn (New York: Wiley)
[3] Tipler P A 1976 *Physics* (New York: Worth Publishers)
[4] Fowles G R 1977 *Analytical Mechanics* 3rd edn (New York: Holt, Rinehart and Winston)
[5] The double pendulum video.
[6] Romer R H 1970 A double pendulum'Art Machine' *Am. J. Phys.* **38** 1116–21
[7] Sinbrot T, Grebogi C, Wisdom J and Yorke J A 1992 Chaos in a double pendulum *Am. J. Phys.* **60** 491–9
[8] Levien R B and Tan S M 1993 Double pendulum: an experiment in chaos *Am. J. Phys.* **61** 1038–44
[9] DeSerio R 2003 Chaotic pendulum: the complete attractor *Am. J. Phys.* **71** 250–7
[10] Cross R 2005 A double pendulum swing experiment: in search of a better bat *Am. J. Phys.* **73** 330–9
[11] Weber J and Wilhelm T 2020 The benefit of computational modelling in physics teaching: a historical overview *Eur. J. Phys.* **41** 034003
[12] Rafat M Z, Wheatland M S and Bedding T R 2009 Dynamics of a double pendulum with distributed mass *Am. J. Phys.* **77** 216–23
[13] Cadwell L H and Boyko E R 1991 Linearization of the simple pendulum *Am. J. Phys.* **59** 979–81
[14] Bender C M and Orszag S A 1978 *Advanced Mathematical Methods for Scientists and Engineers* (New York: McGraw-Hill)
[15] Recktenwald G 2000 *Numerical Methods with MATLAB* (Englewood Cliffs, NJ: Prentice-Hall)
[16] See MATLAB code submitted as supplemental material which was used to numerically solve the governing equations.
[17] D'Alessio S 2020 The magnetic pendulum and weather *Phys. Educ.* **55** 063002
[18] Duchesne B, Fischer C W, Gray C G and Jeffrey K R 1991 Chaos in the motion of an inverted pendulum: an undergraduate laboratory experiment *Am. J. Phys.* **59** 987–92
[19] Wolf A, Swift J B, Swinney H L and Vastano J A 1985 Determining Lyapunov exponents from a time series *Physica* D **16** 285–317
[20] Goldstein H 1980 *Classical Mechanics* (Reading, MA: Addison-Wesley Developers Press)